Chemical Engineering Journal 513 (2025) 162996

Contents lists available at ScienceDirect

Chemical Engineering Journal

journal homepage: www.elsevier.com/locate/cej

Reaction kinetic and application of methane reforming with CO_2/H_2O in flue gas for heat recovery and carbon conversion

Guinan He [a], Haigang Zhang [a], Wencai Zhou [b,c], Hongjie Zeng [b,c], Zhongjie Shen [a,*], Haifeng Liu [a,d,*]

[a] National Energy Coal Gasification Technology Research and Development Center and Shanghai Engineering Research Center of Coal Gasification, East China University of Science and Technology, P. O. Box 272, Shanghai 200237, PR China
[b] Innovation Center for Advanced Glass Materials (Anhui) Co., Ltd., Bengbu 233000, PR China
[c] China Triumph International Engineering Co., Ltd., Shanghai 200063, PR China
[d] Liaoning Petrochemical University, Fushun, Liaoning 113001, PR China

ARTICLE INFO

Keywords:
Flue gas recovery
Methane reforming
Kinetic
Reaction mechanism
Carbon conversion

ABSTRACT

Methane reforming with the flue gas rich in carbon dioxide and steam emitted from industry is an effective method to achieve heat recovery and reduce carbon emission. This study investigated the reaction kinetic and mechanism of methane reforming with CO_2/H_2O in flue gas under various conditions of temperatures, mixing gas ratios, and flow rates. The results show that methane and flue gas can react sufficiently above 1200 °C with a conversion rate exceeding 90 %. Raising methane levels by 16 % boosts hydrogen production by 12 %, while increasing CO_2 by 7 % enhances CO yield by 10 %. The average activation energy for the methane flue gas reforming reaction can be obtained by fitting to the power-law kinetics model, which is 202.8 kJ/mol. Concurrently, by integrating density functional theory (DFT) calculations, the mechanism model for the reforming of methane/flue gas has been derived, which also demonstrates that the carbon black produced from methane pyrolysis can act as a catalyst for the methane reforming reaction. This study aims to a theoretical foundation and process parameters for the design of carbon capture, utilization, and heat recovery from industrial waste flue gas.

1. Introduction

In recent years, fossil fuels such as coal, oil, and natural gas continued to be used as the main energy sources in energy-intensive industries like steel [1], glass [2], and thermal power generation [3]. However, the consumption of these fuels, which leads to the emission of large amounts of greenhouse gases and harmful gases such as carbon dioxide (CO_2), sulfur dioxide (SO_2), and nitrogen oxides (NO_x), is inconsistent with the strategic goals of reducing pollution, achieving carbon neutrality, and promoting a comprehensive green transformation of economic and social development [4]. High-temperature flue gas typically contains significant amounts of carbon dioxide and steam, and the direct emission of these gases can lead to widespread environmental pollution and an increase in average temperatures [5]. For instance, in the glass industry, China emits 0.69 tons of carbon dioxide per ton of glass product, which is significantly higher than the 0.46 tons in the European container glass industry [6]. The main reasons for this difference are China's energy structure, which is mainly based on coal, and the fact that the European glass industry primarily uses natural gas [7]. Another reason for the higher carbon dioxide emissions is China's carbon dioxide recycling rate, which is only 28 %, far below the 65.5 % rate in Europe [8]. Improving the carbon dioxide recycling rate is a major way to reduce carbon emissions without changing the energy structure.

Although carbon dioxide emissions can be managed through existing technologies such as Carbon Capture and Storage (CCS) [9], Carbon Capture and Utilization (CCU) [10], and Direct Air Capture (DAC) [11], the additional costs and carbon losses make the application of these technologies in industry complex. Moreover, the high-temperature flue gas emitted by industries usually has a temperature exceeding 1000 °C [12], and the use of carbon capture technology does not recover the heat from the flue gas, resulting in unnecessary heat loss. For waste heat

* Corresponding authors at: National Energy Coal Gasification Technology Research and Development Center, East China University of Science and Technology, P. O. Box 272, Shanghai 200237, PR China.
E-mail addresses: zjshen@ecust.edu.cn (Z. Shen), hfliu@ecust.edu.cn (H. Liu).

https://doi.org/10.1016/j.cej.2025.162996
Received 4 November 2024; Received in revised form 1 April 2025; Accepted 22 April 2025
Available online 24 April 2025

recovery, preheating the combustion gases to recover waste heat back into the process often has a higher energy efficiency than internal heat use or conversion into other forms of energy [13]. Therefore, a method capable of efficiently capturing carbon and recovering heat from flue gas is needed. Given that the main components of flue gas are carbon dioxide and water vapor, introducing an appropriate amount of methane gas into the flue gas can trigger Dry Methane Reforming (DMR) and Steam Methane Reforming (SMR) reactions with carbon dioxide and water vapor, respectively. This effectively converts carbon dioxide and water vapor into cleaner energy sources such as carbon monoxide and hydrogen [14]. At the same time, the waste heat from the flue gas can provide the heat required for the reforming reaction, thus promoting the progress of the reforming reaction.

In the process of utilizing methane to consume carbon dioxide, steam, and waste heat from flue gas to produce synthesis gas, determining whether the methane flue gas reforming reaction can proceed spontaneously is the most critical step [15]. Methane reforming can mainly be divided into Steam Methane Reforming and Dry Methane Reforming, with reaction equations shown in Eq. (1) and Eq. (2), respectively. The synthesis gas produced by SMR is rich in hydrogen and is thus primarily utilized for large-scale hydrogen production [16]. DMR can directly convert the greenhouse gas carbon dioxide into synthesis gas, increasing the proportion of carbon monoxide in the synthesis gas while also considering the benefit of environmental protection [17]. Nonetheless, both reactions encounter a common issue: being highly endothermic, a substantial amount of heat is required for them to proceed. To address this issue, the introduction of catalysts to reduce the heat required for the reaction or the utilization of plasma technology to generate highly reactive free radicals to promote methane reforming reactions can be employed. For instance, in industry, the use of nickel-based catalysts supported on Al_2O_3 enables methane reforming reactions to proceed at temperatures of 1000–1100 K [18]. Additionally, altering the shape of the catalyst can enhance the methane conversion rate under constant residence time conditions. However, the formation of carbon deposits during methane reforming is almost inevitable. These deposits primarily exist in the form of nanoscale carbon fibers, which can cover the catalyst surface and block the pores, thereby causing catalyst deactivation [19]. In contrast, the high-energy electrons and free radicals generated by plasma technology can excite methane molecules, allowing the reforming reaction to occur at lower temperatures and reducing the problem of carbon deposition [20]. Nevertheless, the high cost of plasma equipment and the instability of the reaction process still pose challenges for large-scale industrial applications. Utilizing high-temperature flue gas as an oxidizing agent can effectively circumvent issues associated with catalysts, with the reaction equation presented in Eq. (3) [21].

$$CH_4 + H_2O \rightarrow CO + 3H_2 \quad \Delta H_R^0 = 206.3\ \text{kJ/mol} \tag{1}$$

$$CH_4 + CO_2 \rightarrow 2CO + 2H_2 \quad \Delta H_R^0 = 247.3\ \text{kJ/mol} \tag{2}$$

$$CH_4 + \frac{2}{3}H_2O + \frac{1}{3}CO_2 \rightarrow \frac{4}{3}CO + \frac{8}{3}H_2 \quad \Delta H_R^0 = 220.0\ \text{kJ/mol} \tag{3}$$

Pre-treating the heat exchanger at high temperature allows the methane reforming reaction to proceed spontaneously without the need for additional heat from the outside or the addition of a catalyst [22]. The spontaneous reforming reaction of methane is accomplished using the thermal energy of high-temperature flue gas [16], thereby recycling the high-temperature flue gas produced industrially [23,24]. Compared with other direct carbon dioxide capture solutions for high-temperature conversion, such as adsorbent-enhanced reactions [25], chemical looping reforming [26], and gas-switching concepts [27], methane flue gas auto-thermal reforming does not require high-temperature and water-resistant adsorbents or stable oxygen carriers. This avoids the high investment costs associated with complex adsorbent regeneration and oxygen carrier circulation systems. Additionally, unlike gas-switching concepts that necessitate precise control of switching times and conditions, the process of methane flue gas auto-thermal reforming is relatively simpler. This method addresses the challenges of cost incurred by the use of catalysts in industry and the heat loss from high-temperature flue gas, thereby enhancing the system's thermal efficiency and reducing fuel consumption [28–30]. Ensuring the sufficient progress of methane flue gas reforming reactions necessitates initially contemplating whether the flue gas heat can satisfy the reaction's demands [31]. Thus, establishing the temperature necessary for the complete reaction of methane flue gas is vital for the spontaneous reforming of methane induced by high-temperature flue gas [32]. The methane pyrolytic reforming process is an intricate chemical system [33]. The steam present in the reaction only meets half the stoichiometric requirement for carbon, predisposing the system to substantial carbon formation [34,35], which in turn affects the ratio of carbon monoxide to hydrogen at the outlet. This deviation affects the subsequent thermal efficiency of syngas combustion in industrial applications. Consequently, undertaking precise quantification of individual reaction proportions and ascertaining the kinetics of reforming reactions within the comprehensive system are essential. Such an analysis is pivotal for the effective and rational management of synthesis gas ratios at the outlet.

Table 1
Methane flue gas reforming experimental conditions.

Condition	Molar flow rate at 25 °C (mmol/min)			Inlet gas ratio			Time (s)
	CH_4 (g)	CO_2 (g)	H_2O (g)	CH_4(g)	CO_2(g)	H_2O (g)	
C1	53.18	21.27	31.89	2.50	1.00	1.50	21.37
C2	35.45	28.36	42.52	1.25	1.00	1.50	21.37
C3	70.91	14.18	21.30	5.00	1.00	1.50	21.37
C4	26.59	10.64	15.94	2.50	1.00	1.50	42.73
C5	17.73	14.18	21.31	1.25	1.00	1.50	42.73
C6	35.45	7.09	10.63	5.00	1.00	1.50	42.73
C7	17.73	7.09	10.63	2.50	1.00	1.50	64.09
C8	11.82	9.45	14.17	1.25	1.00	1.50	64.09
C9	23.64	4.73	7.08	5.00	1.00	1.50	64.09

This study utilized a high-temperature furnace to study the reforming reaction of methane flue gas. The effects of various temperatures, methane flue gas flow rates, and methane/flue gas ratios on the reaction rate and conversion efficiency were examined, yielding the release patterns of the reformed gases. The kinetics of the reforming reaction were analyzed using a power-law kinetic model and the rate equation for the methane flue gas reforming was proposed. Additionally, the catalytic effect of carbon in the methane flue gas reforming reaction was obtained through thermogravimetric analysis and atomic force microscopy. Finally, the mechanism of the methane/flue gas reforming reaction was simulated using density functional theory (DFT). This research can provide a potential theoretical foundation and process parameters for the design of carbon capture, utilization, and heat recovery from industrial waste flue gas.

2. Experimental

2.1. Materials

The composition and temperature of the flue gas used in the experiment were provided by the Innovation Center for Advanced Glass Materials (Bengbu) and China Triumph International Engineering Co., Ltd. (Shanghai), and simulated the actual industrial flue gas components of a full-oxygen combustion glass furnace (with a fixed volumetric flow ratio of carbon dioxide to steam at 2:3). Methane reforming reactivity studies were conducted under reaction temperatures ranging from 800 °C to 1400 °C (with intervals of 100 °C), on nine different flue gas flow rates and compositions. The experimental conditions were shown in Table 1.

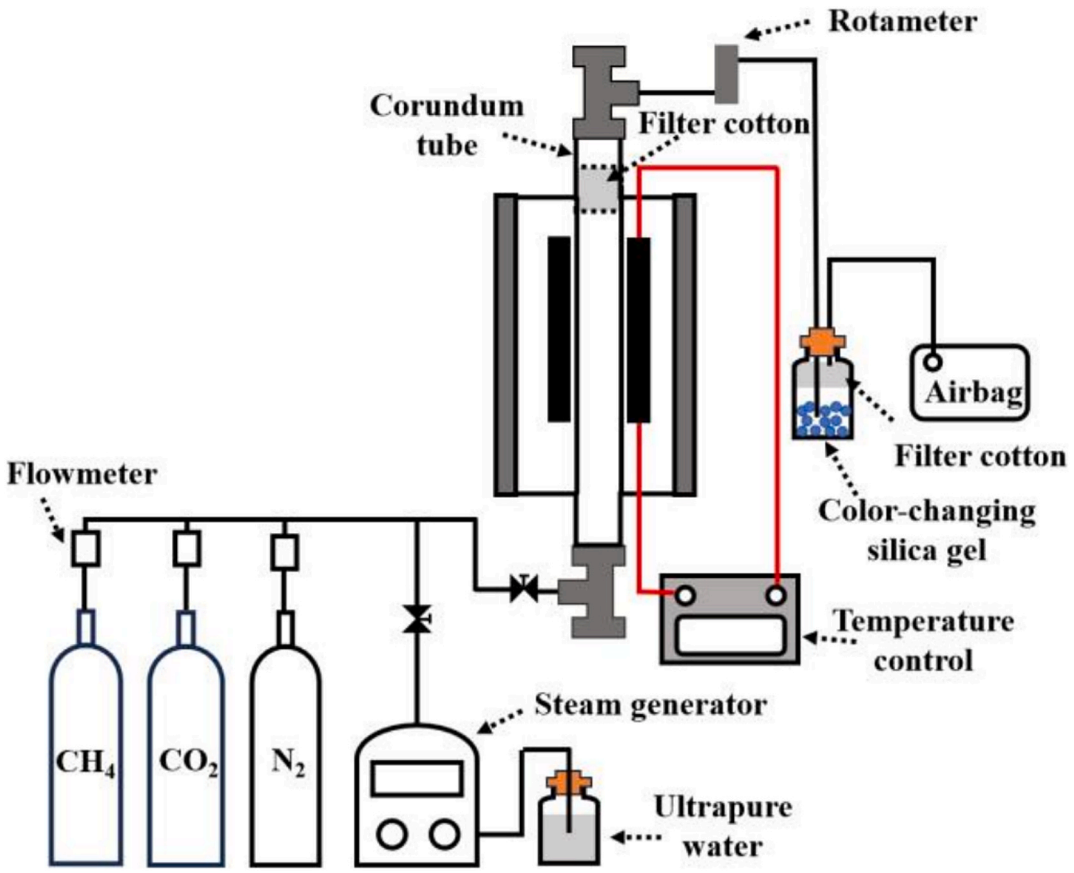

Fig. 1. Methane flue gas thermochemical reforming experimental setup schematic diagram.

The experimental raw materials, including nitrogen, methane, and carbon dioxide, were all sourced from Shanghai Haoqi Company with a purity of 99.99 %. The steam required for the experiment was generated by a steam generator under conditions of 105 °C.

2.2. Experimental procedure

The methane reforming experiment was conducted in an atmospheric pressure tubular furnace, where the tube was an alumina tube resistant to high temperatures (<1600 °C), with a length of 1000 mm and an inner diameter of 60 mm. As shown in Fig. 1, the temperature of the alumina tube was measured using a Type B thermocouple, and the isothermal reforming reaction zone was heated by silicon carbide heating elements. The flow rates of methane, carbon dioxide, and nitrogen used in the reaction were controlled using Digital MFC tools and software. The synthesis gas produced by the reforming reaction was analyzed for gaseous components using a gas chromatograph (Agilent, USA) equipped with a thermal conductivity detector (TCD).

During the heating phase of the apparatus, nitrogen gas was introduced into the alumina tube as a protective gas. The furnace was heated to the setting temperature at a rate of 10 °C/min and then held for 5 min to ensure the temperature of the tubular furnace was uniform. Once the temperature of the tubular furnace was stable, nitrogen was switched to reactive gas to carry out the reforming reaction of methane and flue gas. After 10 min, the reactive gas was ensured to be fully mixed within the gas pipeline before being introduced into the tubular furnace for the reaction. The flow rate of the outlet gas was recorded using a rotameter. The gas, after being dried by color-changing silica gel and filter cotton, was collected in a gas bag for 3 min. Each set of gas was collected and the procedure was repeated three times. After collecting the gas, 200 mL/min of nitrogen was introduced for cooling. When the tube furnace had cooled down to room temperature, the carbon black deposited at the bottom of the tube furnace was collected.

The rate of methane reaction can be calculated according to Eq. (4)

$$v = \frac{q_{in,CH_4} - q_{out} \cdot x_{CH_4}}{22.4 \cdot V} \tag{4}$$

where V represents the volume of the isothermal section of the reactor, L, q_{in,CH_4} is the methane feed rate, L/s, q_{out} is the total outlet gas flow rate, L/s, and x_{CH_4} is the methane content in the outlet gas, %. The methane conversion rate is calculated using Eq. (5)

$$\eta = \frac{q_{in,CH_4} - q_{out} \cdot x_{CH_4}}{q_{in,CH_4}} \tag{5}$$

Additionally, the residence time of the gas in the pipeline can be calculated using Eq. (6).

$$\tau = \frac{1000 \cdot L \cdot A}{q_{in}} \tag{6}$$

where L is the length of the pipe, m, A is the cross-sectional area, m^2, and q_{in} is the total inlet gas flow rate, L/s.

To avert the formation of carbon black in the methane reforming process, the reaction was customarily conducted at elevated temperatures, employing steam and carbon dioxide to deplete the carbon black. Nonetheless, experiments had demonstrated that carbon black was not completely consumed at temperature up to 1400 °C. In order to elucidate the behavior of coke during the methane flue gas reforming process, the gasification reactivity of methane reforming carbon black, collected under condition (1) at 1400 °C, and methane pyrolysis carbon black under the same conditions, was investigated separately using a thermogravimetric analyzer (STA 449 F3, Germany). 10 mg of carbon black was weighed and placed into the thermogravimetric analyzer. A temperature program was set to heat up at a rate of 25 K/min to 105 °C and

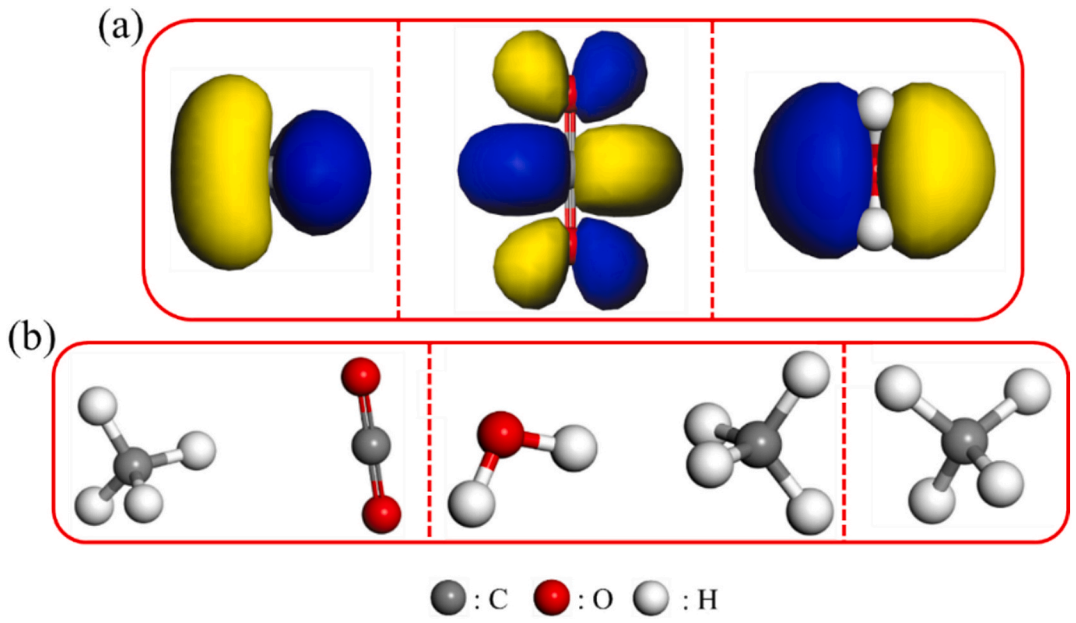

Fig. 2. Orbital and Structural Optimization of Reactants: (a) HOMO of methane and LUMO of carbon dioxide and water vapor, (b) optimized structures of reactants for dry methane reforming, steam methane reforming, and methane cracking.

held for 10 min. Then, the temperature was increased at a rate of 25 K/min to 1350 °C and held for one hour. After the reaction was completed, the temperature was decreased at a rate of 50 K/min to 100 °C. Nitrogen was introduced as a protective gas during the heating process, and high purity carbon dioxide was introduced as the reaction gas to react with the carbon black for gasification during the isothermal period at 1350 °C, to obtain the change rule of carbon black mass loss over time.

Surface activity analysis of collected methane reforming carbon black was conducted using atomic force microscopy (AFM) (Bruker Dimension Icon, Germany). Utilizing the contact mode of atomic force

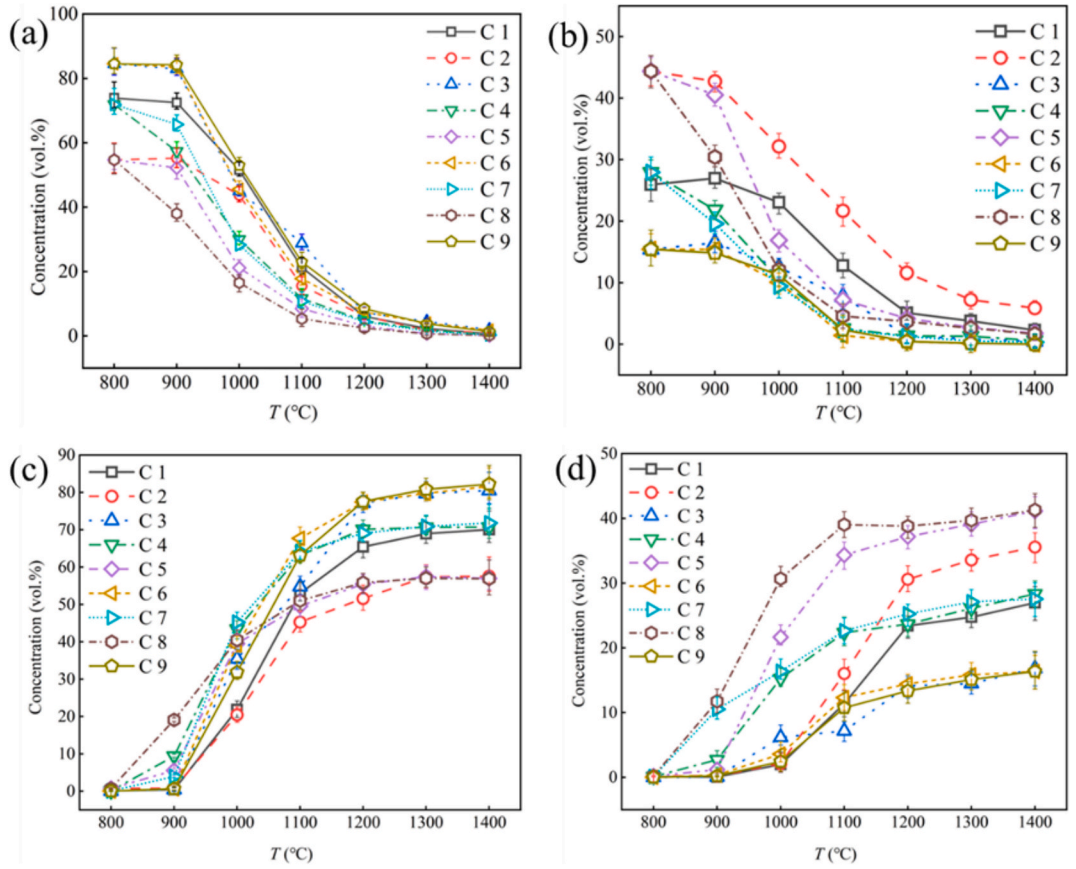

Fig. 3. Composition (volume fraction) of synthetic gas in methane flue gas reforming reaction under different conditions: (a) methane volume fraction, (b) carbon dioxide volume fraction, (c) hydrogen volume fraction and (d) Carbon monoxide volume fraction.

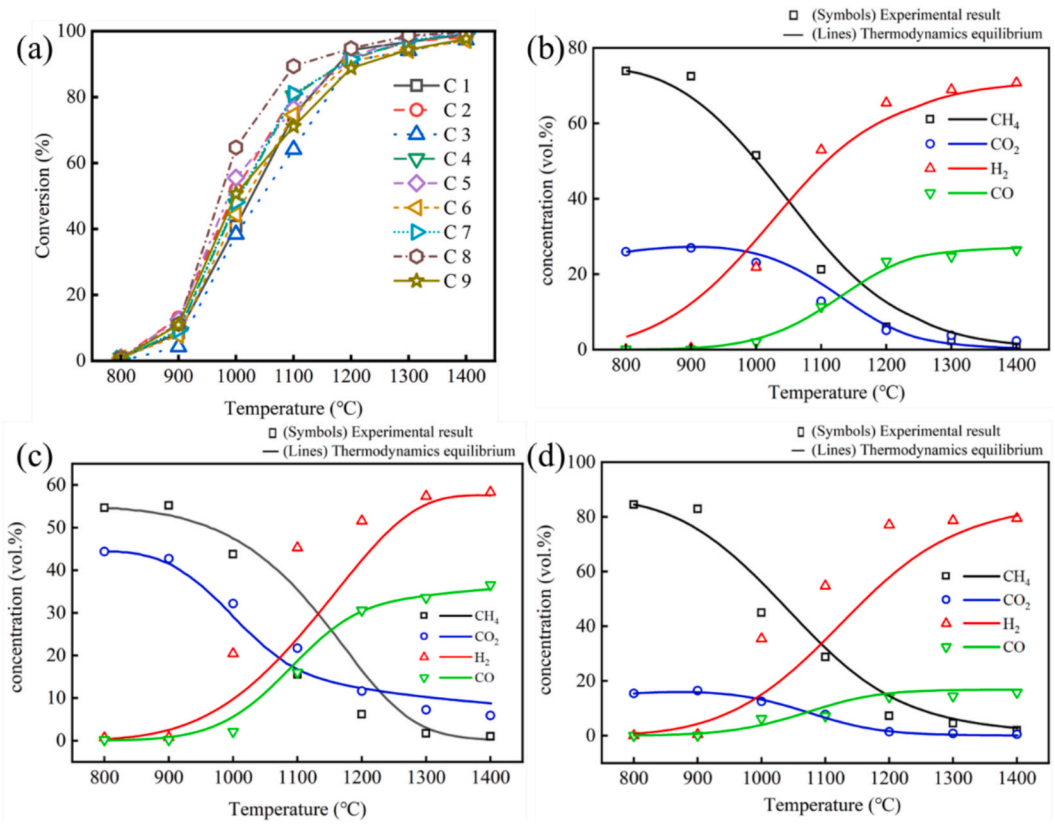

Fig. 4. Methane conversion and thermodynamic equilibrium calculations under different conditions: (a) methane conversion and comparison of thermodynamic equilibrium calculations. Experimental values at different methane to flue gas ratios: (b) CH_4:CO_2:H_2O = 2.5:1:1.5, (c) CH_4:CO_2:H_2O = 1.25:1:1.5 and (d) CH_4:CO_2:H_2O = 5:1:1.5.

microscopy for scanning and performing 50 force curves on the sample surface. Employing the ScanAsyst-Air probe with a reflective Al coating on the back, a resonance frequency of 70 kHz, a spring constant of 0.4 N/m, and a cantilever length of 115 μm.

2.3. Computational methods

The transition state calculations for the methane reforming reaction were performed using the DMol3 module [36] in Accelrys's Materials Studio software, with valence electron wave functions expanded using a double numerical basis set with polarization functions (DNP+) [37]. The complete linear synchronous and quadratic synchronous transformation (complete LST/QST) method [38] was employed to calculate the reaction transition states, and to address the problem of energy overestimation due to ignoring spin polarization, spin polarization was considered in the calculations. In the calculations of the transition states and mechanisms for dry methane reforming and steam methane reforming reactions, a combination of generalized gradient approximation (GGA) and Becke-Perdew (BP) functionals (GGA-BP) [39] was employed. For the calculations of the transition states and mechanisms for methane cracking reactions, the Hartree-Fock (HF) [40] exchange functional was utilized.

According to the Frontier Molecular Orbital Theory, a chemical reaction occurs between the highest occupied molecular orbital (HOMO) of one molecule and the lowest unoccupied molecular orbital (LUMO) of another molecule. Based on this, the orbital energies of methane, carbon dioxide, and water vapor molecules were calculated. The HOMO and LUMO energies of the methane molecule are −18.465 eV and −5.55 eV, respectively. For the carbon dioxide molecule, the HOMO and LUMO energies are −18.551 eV and −10.552 eV, respectively. The HOMO and LUMO energies of the water vapor molecule are −20.849 eV and −17.94 eV, respectively. Since reactions are more likely to occur between the HOMO and LUMO with the smallest energy gap, the dry reforming of methane takes place between the HOMO of methane and the LUMO of carbon dioxide, while the steam reforming of methane occurs between the HOMO of methane and the LUMO of water vapor. The HOMO diagram of methane and the LUMO diagrams of carbon dioxide and water vapor are shown in Fig. 2a. The reactants were placed according to the positions with the largest corresponding areas of the two orbitals, and then structural optimization was performed, with the results shown in Fig. 2b.

3. Results and discussion

3.1. Composition of gaseous products

The results of methane reforming under different conditions are shown in Fig. 3. Under the same inlet gas flow rate, different methane/flue gas ratios have a significant impact on the content of outlet gases from the methane reforming reaction. An increase in the methane content in the feed gas significantly raises the concentration of hydrogen in the product gas, while an increase in carbon dioxide content markedly elevates the concentration of carbon monoxide in the product. For example, comparing condition (1) with condition (2) reveals, when the methane/flue gas ratio is reduced from 1:1 to 1:2, the hydrogen content in the outlet gas decreases from 80.49 % to 70.00 % (at 1400 °C) with the reduction of methane content, and the increase in CO_2 content leads to an increase in carbon monoxide content from 26.96 % to 35.56 % (at 1400 °C). However, under the same methane/flue gas ratio, as the inlet gas flow rate increases, i.e., the reaction residence time increases, the content of outlet gas components remains essentially unchanged. For example, comparing the outlet gas results of conditions (1), 4, and 7

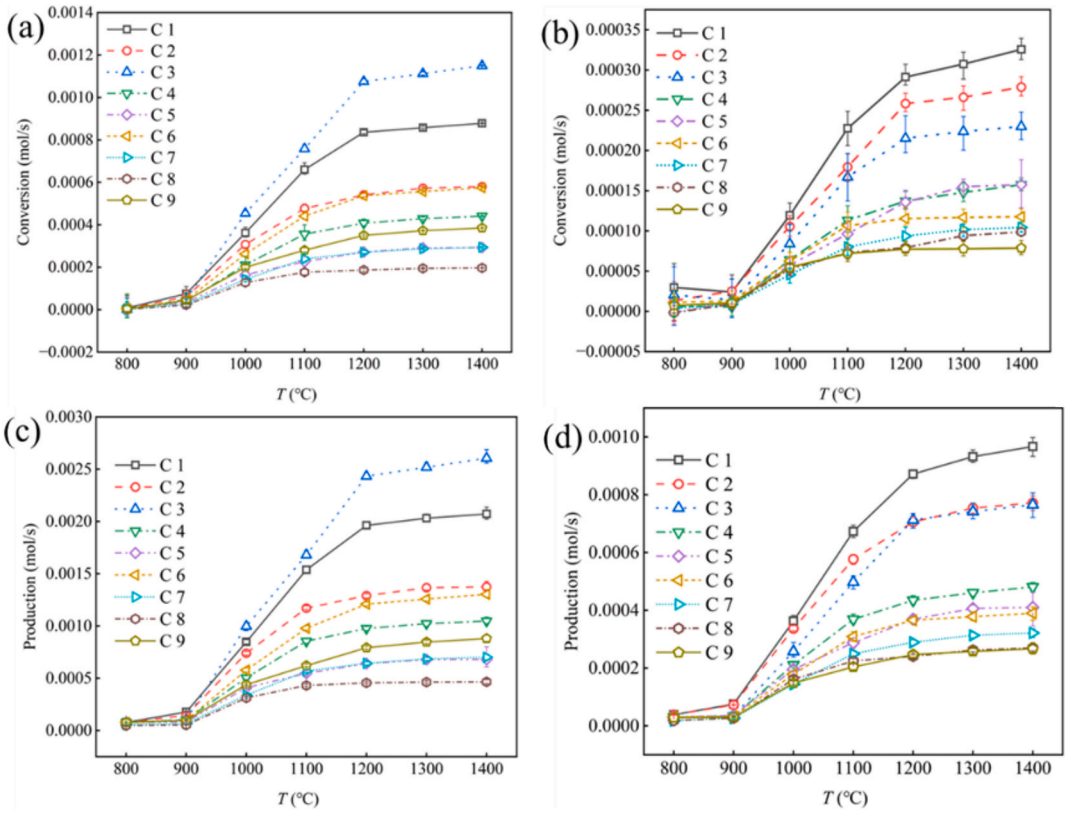

Fig. 5. The change in the quantities of substances during methane reforming under various conditions: (a) methane conversion, (b) carbon dioxide conversion, (c) hydrogen production and (d) carbon monoxide production.

shows that at 1400 °C, with the increase in inlet gas flow rate, i.e., the increase in residence time, the hydrogen content in the outlet gas for the three conditions is 70.04 %, 70.69 %, and 71.80 % respectively, and the carbon monoxide content is 26.96 %, 28.32 %, and 27.54 % respectively. This may be due to the fact that when the residence time is 21.36 s, the methane reforming reaction has reached an equilibrium phase. Therefore, further increasing the inlet flow rate of methane and flue gas has a minimal impact on the content of hydrogen and carbon monoxide in the outlet gas.

The variation of methane conversion rate with temperature under different conditions is shown in Fig. 4a. Observing that the methane conversion rate remains essentially constant under different methane/flue gas ratios and inlet gas flow rates. However, as the temperature increases, there is a significant increase in the methane conversion rate, especially between 800–1200 °C, where the methane conversion rate increases dramatically from an initial 1 % to over 90 %. When the temperature is further raised to 1300 °C and 1400 °C, the methane conversion rate remains essentially unchanged, indicating that the methane reforming reaction has essentially reached equilibrium at 1200 °C. Fig. 4b–d presents the thermodynamic equilibrium calculations and experimental results for the outlet gas composition (including methane, carbon dioxide, hydrogen, and carbon monoxide) under different methane to flue gas ratios. The thermodynamic equilibrium calculations were primarily based on the method for thermodynamic equilibrium analysis of methane dual reforming under catalytic conditions as reported in the literature [16]. The results show a high degree of consistency between the calculated and experimental values. However, a significant discrepancy in the hydrogen yield is mainly attributed to the substantial contribution of methane cracking reactions at high temperatures, resulting in higher hydrogen content in the experimental results than in the theoretical calculations.

Combining the above results of methane flue gas reforming outlet gas content under different conditions, altering the methane/flue gas ratio in the inlet gas changes the hydrogen and carbon monoxide content in the outlet gas, adjusting the composition of the outlet gas. Increasing the temperature can enhance the reaction rate of the methane reforming reaction and the methane conversion rate, thereby increasing the content of hydrogen and carbon monoxide in the outlet gas. Compared with adsorbent-enhanced reactions, chemical looping reforming, and gas-switching concepts, methane flue gas reforming can achieve high carbon conversion rates and reaction rates even at higher temperatures. Meanwhile, methane flue gas reforming is also capable of producing a relatively high yield of hydrogen.

3.2. *Reforming and pyrolysis reaction proportions*

Based on the volumetric fractions of methane, carbon dioxide, hydrogen, and carbon monoxide in the outlet gas, combined with the outlet gas flow rate and the molar amounts of methane and carbon dioxide in the inlet gas, the reaction amounts of methane and carbon dioxide, as well as the generation amounts of hydrogen and carbon monoxide, can be calculated, with the results shown in Fig. 5. Under the same inlet gas flow rate, the generation of hydrogen in the outlet gas is primarily influenced by the partial pressure of methane; the higher the partial pressure of methane, the higher the hydrogen content in the outlet gas. This is associated with the cracking of methane to produce hydrogen. In contrast, the generation of carbon monoxide in the outlet gas is not entirely determined by the partial pressure of flue gas. For instance, compared with condition (1), condition (2) has a significantly higher conversion of carbon dioxide, yet the content of carbon monoxide in the outlet gas is roughly the same. This is mainly because the excessively low partial pressure of methane is insufficient to completely react with the flue gas. Therefore, appropriately increasing the partial pressure of methane enhances the hydrogen content and boosts the carbon monoxide content. However, an excessively high methane proportion can also reduce the yield of carbon monoxide. For example, compared

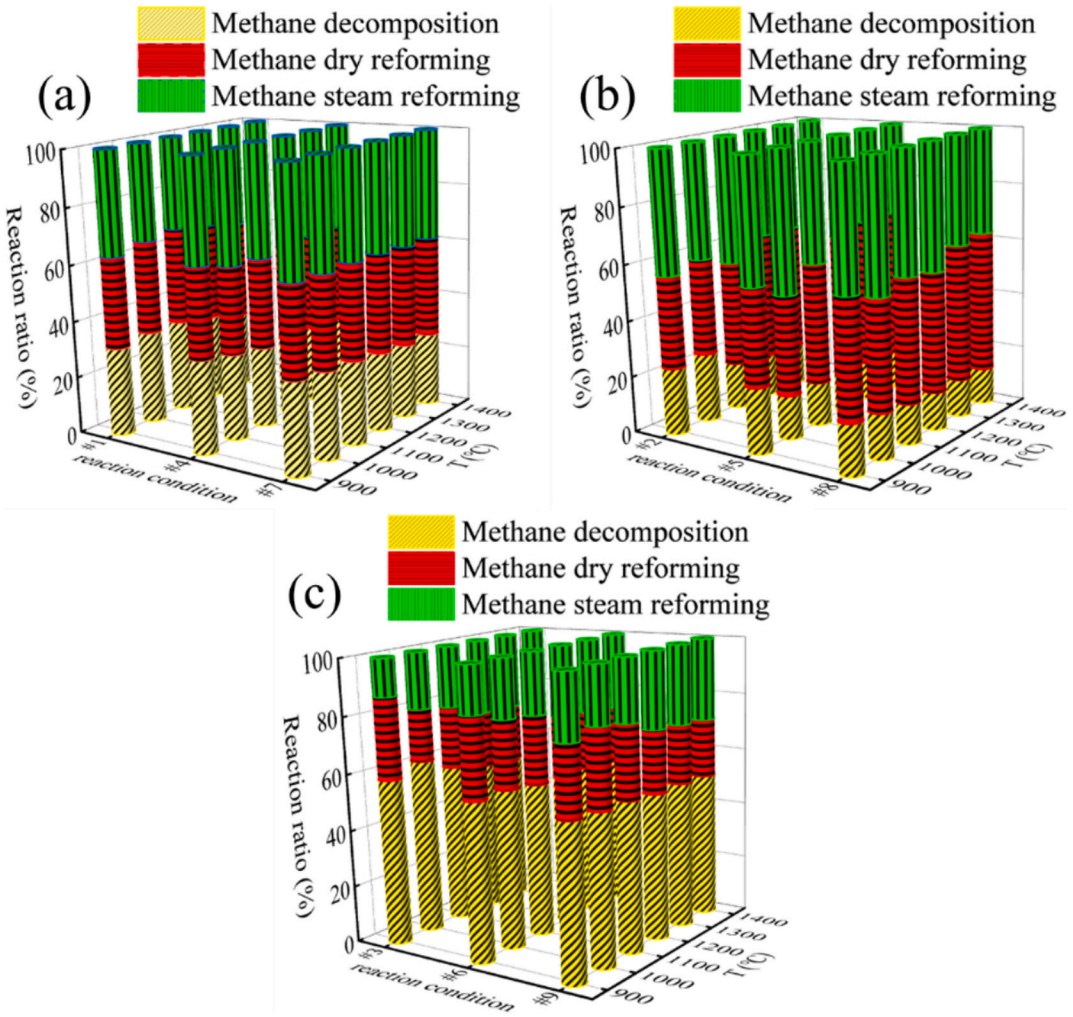

Fig. 6. The proportion of each reaction at different flows and temperatures: (a) methane/flue gas ratio 1:1, (b) methane/flue gas ratio 1:2 and (c) methane/flue gas ratio 2:1.

with condition (1), the higher methane proportion in condition (3), although enhances the hydrogen yield, also leads to a decrease in the carbon monoxide yield. This is primarily because an overly high methane proportion tends to promote the methane cracking reaction, which in turn brings about a more severe carbon deposition issue. Therefore, maintaining the ratio of methane to flue gas at 1:1 can maximize the yield of synthesis gas. Under the same methane/flue gas ratio conditions, appropriately increasing the inlet flow rate of methane and flue gas will increase the flow rates of hydrogen and carbon monoxide in the outlet gas. According to the reaction equations of dry reforming and steam reforming, all the reacted carbon dioxide is converted into carbon monoxide, while the excess generation of carbon monoxide comes entirely from the methane steam reforming.

Based on the molar quantities of reactants and products transformed, the ratios of the reaction amounts of various substances can be determined, thereby obtaining the proportions of methane pyrolysis, dry reforming of methane, and steam reforming of methane in the reaction process. The calculation method is as follows: since the reaction hardly occurs at 800 °C, the temperature range for calculation is 900–1400 °C. Based on the aforementioned reaction amounts of methane and carbon dioxide, as well as the generation amounts of hydrogen and carbon monoxide, the ratios of each reactant and product to methane can be obtained. Assuming a methane consumption rate of 1 mol/s, the consumption of methane can be calculated based on the stoichiometric coefficients of the reactions of methane pyrolysis, dry reforming of methane, and steam reforming of methane. Thereby, the proportions of the three reactions in the entire reaction process can be obtained, with the results shown in Fig. 6. With the increase of temperature, the proportion of methane pyrolysis decreases, while both steam reforming and dry reforming of methane increase. At a methane/flue gas ratio of 1:1, as shown in conditions (1), 4, and 7, the proportions of the three reactions are relatively balanced, but compared to the other two reactions, steam reforming of methane occupies a larger proportion, indicating that steam reforming of methane is more likely to occur. When the methane/flue gas ratio is 1:2, as shown in conditions (2), 5, and 8, the reactions are mainly dry reforming and steam reforming of methane. At low temperatures below 1100 °C, the proportion of steam reforming of methane is higher than that of dry reforming, but when the temperature exceeds 1100 °C, the proportion of dry reforming becomes higher than that of steam reforming, indicating that at higher flue gas ratios, temperature has a greater impact on dry reforming of methane. However, when the methane/flue gas ratio is 2:1, as shown in conditions (3), 6, and 9, due to the excess of methane, the reaction is mainly methane pyrolysis, and at low temperatures below 1100 °C, the proportion of dry reforming is higher than that of steam reforming. When the temperature exceeds 1100 °C, the proportion of steam reforming becomes higher than that of dry reforming, which is the opposite of when flue gas is in excess, indicating that at higher methane ratios, temperature has a greater impact on steam reforming of methane.

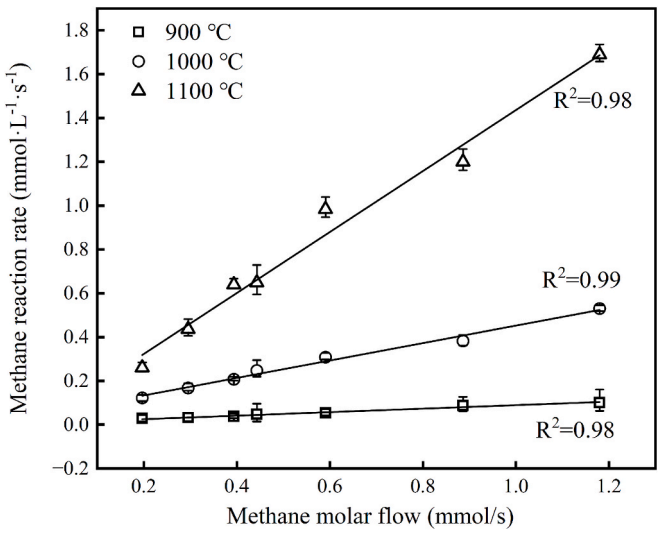

Fig. 7. Diagram of methane reaction rate with flow rate.

3.3. Reforming reaction kinetics analysis

Calculations from the aforementioned reaction equations indicate that the methane flue gas reforming process includes dry reforming of methane, steam reforming of methane, and methane pyrolysis. Therefore, in determining the overall reaction rate, consideration must be given to the collective impact of these reactions. Fig. 7 illustrates the relationship between the methane flow rate and the methane reaction rate within the temperature range of 900–1100 °C. The figure demonstrates a direct proportionality between the methane flow rate and the reaction rate, suggesting a first-order reaction with respect to methane in the methane flue gas reforming process. Additionally, based on the calculated reaction quantities of methane, carbon dioxide, and steam, the reaction orders for carbon dioxide and steam can be determined. To obtain the overall rate equation for the reaction, the methane reforming rate is used to represent the rates of the three main reactions in the methane flue gas reforming, employing a power function-type kinetic equation as shown in Eq. (7). Since the reaction reaches equilibrium at 1200 °C, the calculation of the methane reaction rate covers a temperature range of 800–1200 °C.

$$r_{CH_4} = K\cdot[CH_4]\cdot[CO_2]^a\cdot[H_2O]^b \quad (7)$$

where r_{CH4} represents the reaction rate of methane with units of mol/(L·s), K denotes the rate constant, which can be expressed using the Arrhenius equation ($K = A\cdot e^{-Ea/RT}$), $[CH_4]$, $[CO_2]$ and $[H_2O]$ represent the molar flow rates of methane, carbon dioxide, and steam, respectively, mol/s. The variables a and b represent the reaction orders with respect to carbon dioxide and steam, respectively.

Fig. 8 illustrates the trend of methane reaction rate variation with temperature under different methane/flue gas ratios from 800 to 1200 °C. As shown in the figure, the logarithm of the methane reaction rate exhibits a linear change with temperature. The activation energy (Ea) and pre-exponential factor (A) for the methane reforming reaction can be determined from the slope and intercept values. At the same inlet gas flow rate, a lower methane ratio leads to a certain decrease in the rate of methane reforming reaction. The increase in the inlet gas flow rate results in a noticeable increase in the methane reforming reaction rate, but the overall activation energy of the reaction remains essentially unchanged. This is also consistent with the aforementioned calculations of the proportions of each reaction, indicating that under the condition of the same methane/flue gas ratio, the reaction proportions between

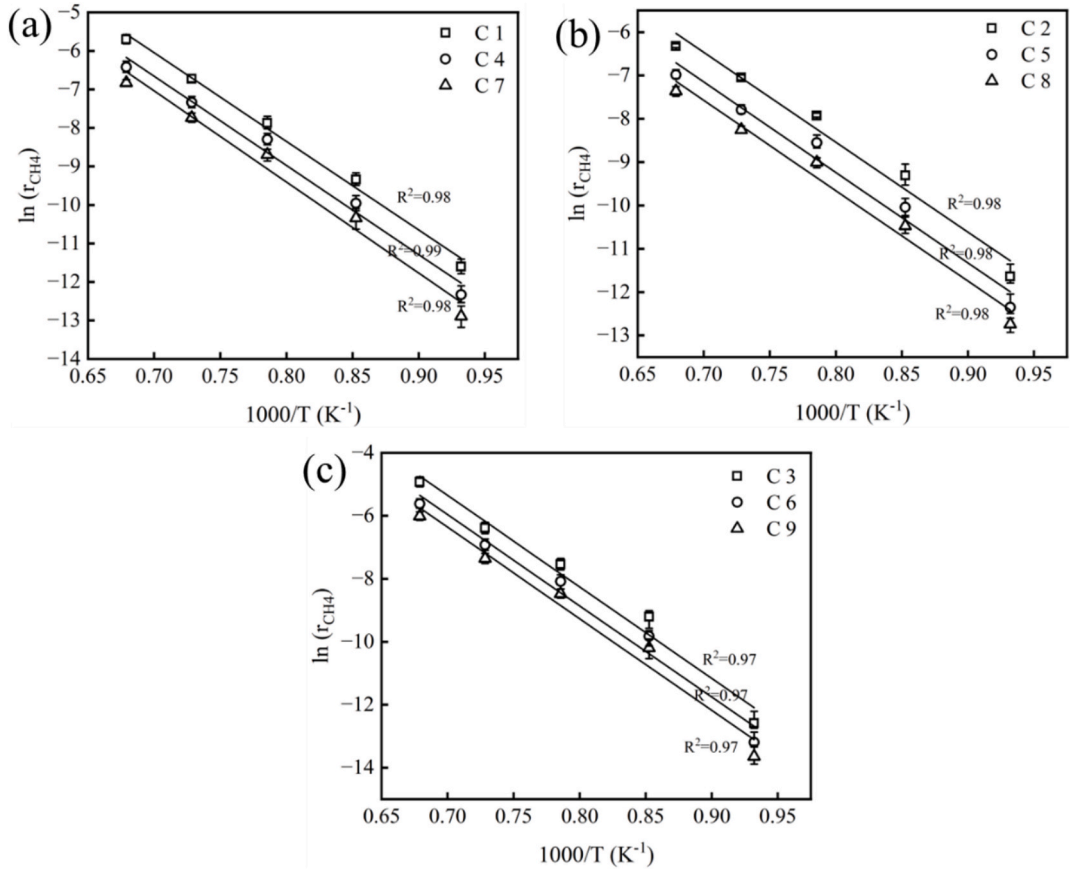

Fig. 8. Activation energy of methane flue gas reforming reaction: (a) methane/flue gas ratio 1:1, (b) methane/flue gas ratio 1:2 and (c) methane/flue gas ratio 2:1.

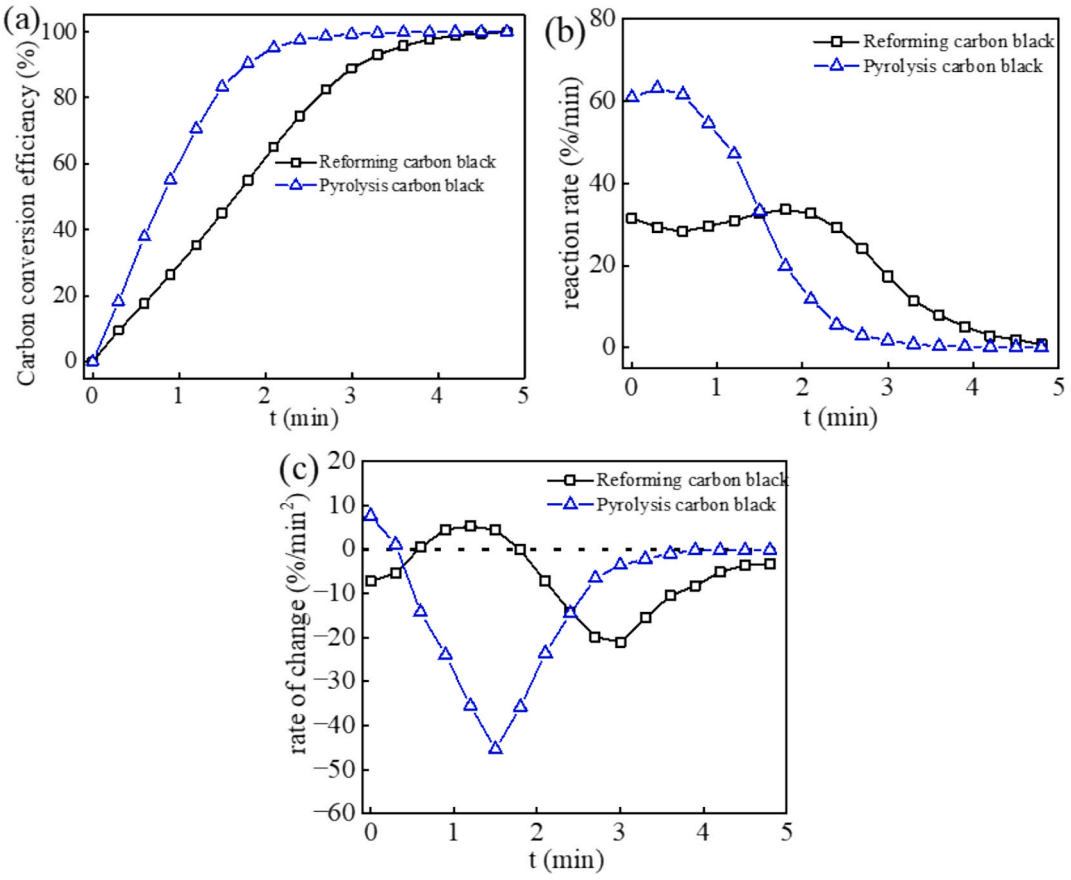

Fig. 9. Thermogravimetric results of methane reforming carbon black and methane pyrolysis carbon black: (a) TG curve of carbon black, (b) DTG curve of carbon black and (c) gasification rate change curve of carbon black.

methane pyrolysis, dry reforming of methane, and steam reforming of methane do not change with the variation of inlet gas flow rate. The average reaction rate equation for methane flue gas reforming is as shown in Eq. (8).

$$r_{CH_4} = 2.1 \times 10^{11} \cdot e^{-202.8/RT} \cdot [CH_4] \cdot [CO_2]^{0.3} \cdot [H_2O]^{0.4} \quad (8)$$

3.4. Stability and surface activity analysis of carbon black

At 1350 °C, the thermogravimetric analysis results of methane reforming carbon black and methane pyrolysis carbon black are presented in Fig. 9. The carbon conversion rate curve in Fig. 9a indicates that the complete gasification of methane reforming char and methane pyrolysis char requires 270 s and 180 s, respectively. Therefore, within the short residence time in the high-temperature furnace, complete gasification of char cannot be achieved, leaving residual char in the furnace. This outcome is consistent with the previously mentioned computational results regarding the proportion of methane pyrolysis reactions.

Furthermore, the analysis of Fig. 9b and c, which depict the variation in gasification reaction rate and the rate of change of the gasification reaction rate, reveals that methane reforming carbon black has a lower gasification reaction rate compared to methane pyrolysis carbon black.

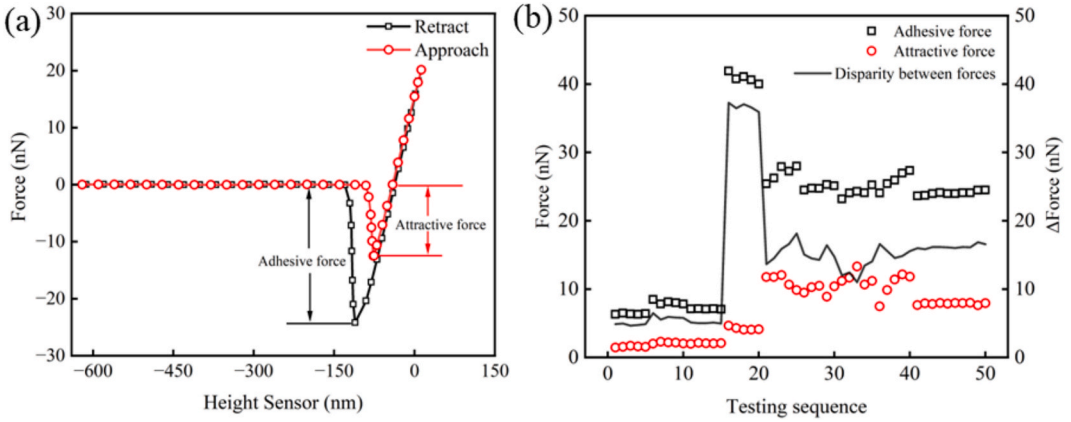

Fig. 10. Methane reforming carbon deposition force curve chart: (a) schematic diagram of carbon black force curve, (b) carbon black attractive-adhesive force distribution graph.

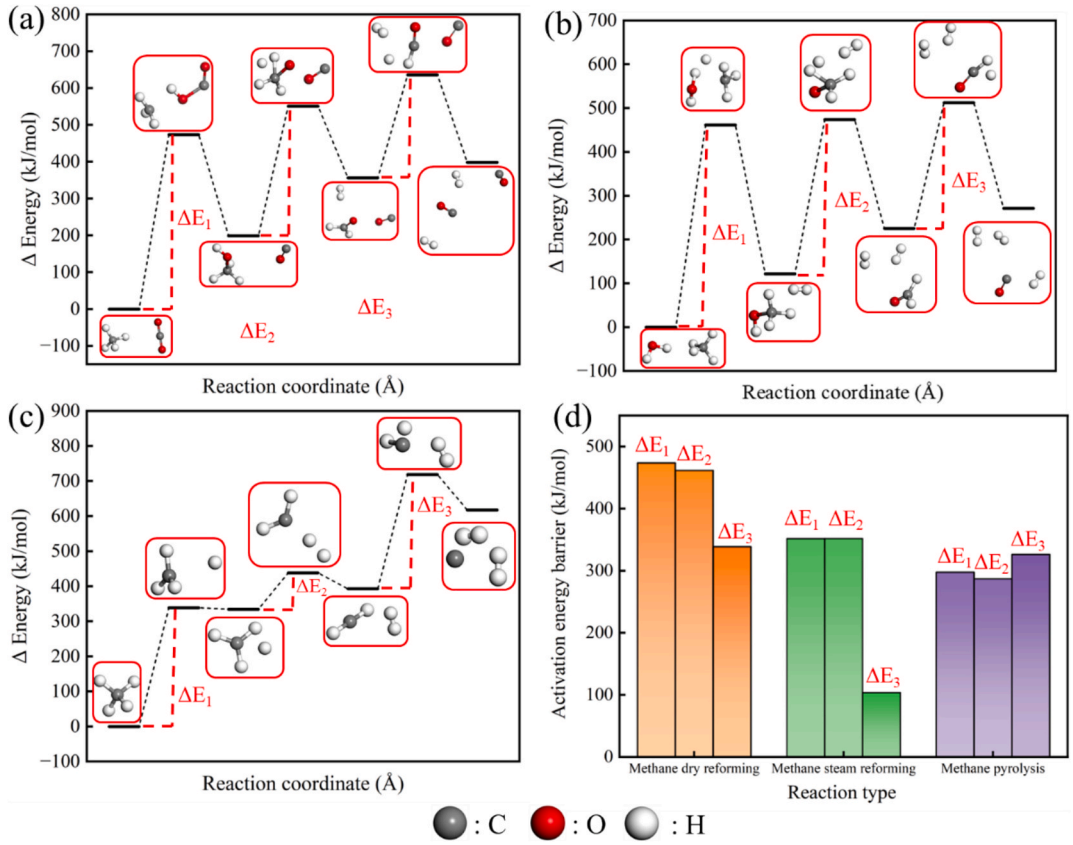

Fig. 11. The mechanism of methane/flue gas reforming reaction: (a) the mechanism of dry reforming of methane reaction, (b) the mechanism of steam reforming of methane reaction and (c) the mechanism of pyrolysis of methane reaction, (d) methane reforming energy distribution.

This indicates that during the methane flue gas reforming process, the more reactive amorphous carbon fraction produced by methane pyrolysis reacts with carbon dioxide and steam, achieving an activation effect, thereby reducing the reactivity of the carbon black. In addition, during the gasification process, the reaction rate of methane reforming carbon black maintains a constant level. This indicates that methane reforming carbon black has a very low reactivity after undergoing the reforming reaction. The stable nature of methane reforming carbon black can readily cause the deactivation of catalysts.

The force curve derived from the pyrolysis of methane carbon black is depicted in Fig. 10a. Utilizing this curve, the adsorption and desorption forces of the carbon black were computed, with corresponding results illustrated in Fig. 10b. The desorption force distribution is relatively broad, spanning from 6.31 nN to 27.99 nN. This variability implies a dispersed arrangement of active functional groups across the carbon black surface, with higher desorption forces at sites of greater activity and lower forces at sites of lesser activity. The mean values of adsorption and desorption forces for the carbon black are recorded as 7.2 nN and 19.07 nN, respectively. The disparity between these forces is calculated to be 11.87 nN, significantly exceeding that of the N234 catalytic carbon black, which is 6.926 nN [41]. This substantial difference in force suggests the promising potential of methane pyrolysis carbon black as a catalyst in the reforming reactions of methane/flue gas.

3.5. Reforming reaction mechanism analysis

Through the aforementioned analysis, the reforming of methane flue gas mainly consists of three reactions: dry reforming of methane, steam reforming of methane, and pyrolysis of methane, with an average ratio of 1:1:1 among them. Prior research has shown that in the presence of steam and carbon dioxide, methane can potentially react directly with steam or carbon dioxide to form methanol [42,43]. Thus, considering methanol as an intermediate in the reforming reactions, a transition state search was conducted for the dry reforming and steam reforming of methane, as shown in Fig. 11. The energy of the products from methane reforming and pyrolysis is significantly higher than that of the reactants, indicating that the reforming of methane flue gas is an endothermic reaction. From Fig. 11d, the activation barrier ΔE_1 for methanol production from methane reforming is markedly higher than that of the subsequent reactions. This suggests that activating carbon dioxide and methane is the rate-determining step in dry reforming of methane. Furthermore, the activation of methane to a methyl group is identified as the rate-limiting step in steam reforming of methane. Additionally, as shown in Fig. 11c depicting the reaction mechanism of methane

Table 2
Steps and activation energies of methane/flue gas reforming reaction.

Reaction	Reaction steps	Activation energy barrier (kJ/mol)
Dry reforming of methane	$CH_4 + CO_2 \rightarrow CH_3OH + CO$	473.63
	$CH_3OH + CO \rightarrow CH_2O + CO + H_2$	351.63
	$CH_2O + CO + H_2 \rightarrow 2\,CO + 2\,H_2$	297.66
Steam reforming of methane	$CH_4 + H_2O \rightarrow CH_3OH + H_2$	461.57
	$CH_3OH + H_2 \rightarrow CH_2O + 2\,H_2$	351.74
	$CH_2O + 2\,H_2 \rightarrow CO + 3\,H_2$	287.01
Methane pyrolysis reaction	$CH_4 \rightarrow CH_3 + H$	338.79
	$CH_3 + H \rightarrow CH_2 + H_2$	103.63
	$CH_2 + H_2 \rightarrow C + 2\,H_2$	326.13

pyrolysis, the activation barrier ΔE_1 for the activation of methane is also higher than that of the subsequent reactions. This confirms that the activation of carbon dioxide and methane is the rate-limiting step in the overall reforming of methane flue gas.

The reforming of methane/flue gas reaction involves several steps, and the reaction barriers are listed in Table 2. The highest reaction barriers for dry reforming and steam reforming of methane are 473.63 kJ/mol and 461.57 kJ/mol, respectively, both of which are higher than the maximum reaction barrier of 338.79 kJ/mol for methane pyrolysis. Based on the kinetic analysis of the aforementioned methane flue gas reforming reactions, reducing the proportion of methane pyrolysis is beneficial for decreasing the activation energy of the methane flue gas reforming reaction. This implies that the maximum reaction barrier for methane pyrolysis should be higher than that for methane reforming reactions, which contradicts the results obtained from simulation calculations. However, combining the analysis from the experiments on the surface activity of methane pyrolysis carbon black leads to the conclusion that this type of carbon black has strong surface activity and a high catalytic potential. This indicates that during the methane flue gas reforming reaction process, the carbon black produced from methane pyrolysis has a certain catalytic effect on the methane reforming reaction, thereby reducing the maximum reaction barrier for methane reforming.

4. Conclusion

This study investigated the composition of syngas from methane/flue gas reforming and the characteristics of reaction kinetics under conditions of varying methane flue gas ratios and methane flue gas flow rates at temperatures ranging from 800-1400 °C. The results indicate that below 900°C, no significant thermochemical reforming reaction takes place between methane and flue gas. At a reaction temperature of 1200 °C, the reforming of methane and flue gas can proceed sufficiently, with a methane conversion rate exceeding 90 %. Altering the ratios of methane and carbon dioxide can effectively influence the composition of hydrogen and carbon monoxide in the synthesis gas. Raising methane levels by 16 % boosts hydrogen production by 12 %, while increasing CO_2 by 7 % enhances CO yield by 10 %. Based on the power-law kinetics model, the average rate equation for methane flue gas reforming is derived, with an average activation energy of 202.8 kJ/mol. Through density functional theory (DFT) calculations, the mechanism model for the reforming of methane/flue gas has been established. Finally, the catalytic role of carbon black generated from methane pyrolysis in the methane reforming reaction is confirmed by analyzing the stability and surface activity of the carbon black. This study aims to provide the theoretical basis and process parameters for the thermochemical regeneration technology of all-oxygen fired glass melting furnaces, as well as to offer technical references for the design of carbon utilization, and heat recovery from a broader range of industrial waste gases.

5. Print declaration

All figures are color in online version and black/white in print.

CRediT authorship contribution statement

Guinan He: Writing – review & editing, Writing – original draft, Visualization, Resources, Methodology, Investigation, Formal analysis, Data curation. **Haigang Zhang:** Validation, Methodology, Formal analysis, Conceptualization. **Wencai Zhou:** Validation, Supervision, Methodology, Formal analysis, Conceptualization. **Hongjie Zeng:** Validation, Methodology, Formal analysis, Conceptualization. **Zhongjie Shen:** Writing – review & editing, Supervision, Software, Project administration, Methodology, Funding acquisition, Formal analysis, Conceptualization. **Haifeng Liu:** Writing – review & editing, Validation, Supervision, Methodology, Formal analysis, Conceptualization.

Declaration of competing interest

The authors declare that they have no known competing financial interests or personal relationships that could have appeared to influence the work reported in this paper.

Acknowledgments

This study is supported by the National Natural Science Foundation of China (22378130), the Fundamental Research Funds of the Central Universities (2022ZFJH004).

Data availability

The authors are unable or have chosen not to specify which data has been used.

References

[1] C. Fan, R. Wei, T. Cheng, R. Sun, H. Zhang, H. Long, The positive contributions of steel slag in reducing carbon dioxide emissions in the steel industry: Waste heat recovery, carbon sequestration, and resource utilization, Chem. Eng. J. 498 (2024) 155379, https://doi.org/10.1016/j.cej.2024.155379.

[2] H. Li, W. Bao, C. Xiu, Y. Zhang, H. Xu, Energy conservation and circular economy in China's process industries, Energy 35 (2010) 4273–4281, https://doi.org/10.1016/j.energy.2009.04.021.

[3] J.D. McTigue, J. Castro, G. Mungas, N. Kramer, J. King, C. Turchi, G. Zhu, Hybridizing a geothermal power plant with concentrating solar power and thermal storage to increase power generation and dispatchability, Appl. Energy 228 (2018) 1837–1852, https://doi.org/10.1016/j.apenergy.2018.07.064.

[4] M. Filonchyk, M.P. Peterson, L. Zhang, V. Hurynovich, Y. He, Greenhouse gases emissions and global climate change: Examining the influence of CO_2, CH_4, and N_2O, Sci. Total Environ. 935 (2024) 173359, https://doi.org/10.1016/j.scitotenv.2024.173359.

[5] I. Larki, A. Zahedi, M. Asadi, M.M. Forootan, M. Farajollahi, R. Ahmadi, A. Ahmadi, Mitigation approaches and techniques for combustion power plants flue gas emissions: a comprehensive review, Sci. Total Environ. 903 (2023) 166108, https://doi.org/10.1016/j.scitotenv.2023.166108.

[6] A. Schmitz, J. Kamiński, B. Maria Scalet, A. Soria, Energy consumption and CO_2 emissions of the European glass industry, Energy Policy 39 (2011) 142–155, https://doi.org/10.1016/j.enpol.2010.09.022.

[7] D. Guan, J. Meng, D.M. Reiner, N. Zhang, Y. Shan, Z. Mi, S. Shao, Z. Liu, Q. Zhang, S.J. Davis, Structural decline in China's CO_2 emissions through transitions in industry and energy systems, Nature Geosci. 11 (2018) 551–555, https://doi.org/10.1038/s41561-018-0161-1.

[8] M. Zier, P. Stenzel, L. Kotzur, D. Stolten, A review of decarbonization options for the glass industry, Energy Convers. Manage. X 10 (2021) 100083, https://doi.org/10.1016/j.ecmx.2021.100083.

[9] M. Ishaq, I. Dincer, A novel cryogenic-thermochemical approach for clean hydrogen production from industrial flue gas streams with carbon capture and storage, Energ. Conver. Manage. 319 (2024) 118955, https://doi.org/10.1016/j.enconman.2024.118955.

[10] D. Baskaran, P. Saravanan, L. Nagarajan, H.-S. Byun, An overview of technologies for capturing, storing, and utilizing carbon dioxide: technology readiness, large-scale demonstration, and cost, Chem. Eng. J. 491 (2024) 151998, https://doi.org/10.1016/j.cej.2024.151998.

[11] H. Bouaboula, J. Chaouki, Y. Belmabkhout, A. Zaabout, Comparative review of Direct air capture technologies: from technical, commercial, economic, and environmental aspects, Chem. Eng. J. 484 (2024) 149411, https://doi.org/10.1016/j.cej.2024.149411.

[12] D. Pashchenko, I. Karpilov, M. Polyakov, S.K. Popov, Techno-economic evaluation of a thermochemical waste-heat recuperation system for industrial furnace application: operating cost analysis, Energy 295 (2024) 131040, https://doi.org/10.1016/j.energy.2024.131040.

[13] L.R. de Araújo, A.P. Morawski, M.A. Barone, H.R.O. Rocha, J.L.M. Donatelli, J.J.C. S. Santos, Response surface methods based in artificial intelligence for superstructure thermoeconomic optimization of waste heat recovery systems in a large internal combustion engine, Energ. Conver. Manage. 271 (2022) 116275, https://doi.org/10.1016/j.enconman.2022.116275.

[14] X. Zhao, S. Sun, Y. Wang, Y. Zhang, Y. Zhu, B. Zong, J. Hu, P. Williams, C. Wu, The role of reverse Boudouard reaction during integrated CO_2 capture and utilisation via dry reforming of methane, Chem. Eng. J. 491 (2024) 151668, https://doi.org/10.1016/j.cej.2024.151668.

[15] A. Hornung, H. Jahangiri, M. Ouadi, C. Kick, L. Deinert, B. Meyer, J. Grunwald, R. Daschner, A. Apfelbacher, M. Meiller, S. Eder, Thermo-Catalytic Reforming (TCR) – an important link between waste management and renewable fuels as part of the energy transition, Appl. Energy Combust. Sci. 12 (2022) 100088, https://doi.org/10.1016/j.jaecs.2022.100088.

[16] W.-J. Jang, D.-W. Jeong, J.-O. Shim, H.-M. Kim, H.-S. Roh, I.H. Son, S.J. Lee, Combined steam and carbon dioxide reforming of methane and side reactions:

thermodynamic equilibrium analysis and experimental application, Appl. Energy 173 (2016) 80–91, https://doi.org/10.1016/j.apenergy.2016.04.006.
[17] A.H.K. Owgi, A.A. Jalil, I. Hussain, N.S. Hassan, H.U. Hambali, T.J. Siang, D.V. N. Vo, Catalytic systems for enhanced carbon dioxide reforming of methane: a review, Environ. Chem. Lett. 19 (2021) 2157–2183, https://doi.org/10.1007/s10311-020-01164-w.
[18] D. Pashchenko, Experimental study of methane reforming with products of complete methane combustion in a reformer filled with a nickel-based catalyst, Energ. Conver. Manage. 183 (2019) 159–166, https://doi.org/10.1016/j.enconman.2018.12.102.
[19] D. Pashchenko, I. Makarov, Carbon deposition in steam methane reforming over a Ni-based catalyst: experimental and thermodynamic analysis, Energy 222 (2021) 119993, https://doi.org/10.1016/j.energy.2021.119993.
[20] J. Feng, X. Sun, Z. Li, X. Hao, M. Fan, P. Ning, K. Li, Plasma-assisted reforming of methane, Adv. Sci. 9 (2022) 2203221, https://doi.org/10.1002/advs.202203221.
[21] G.A. Olah, A. Goeppert, M. Czaun, G.K.S. Prakash, Bi-reforming of methane from any source with steam and carbon dioxide exclusively to metgas (CO–2 H_2) for methanol and hydrocarbon synthesis, J. Am. Chem. Soc. 135 (2013) 648–650, https://doi.org/10.1021/ja311796n.
[22] J. Richter, F. Rachow, J. Israel, N. Roth, E. Charlafti, V. Günther, J.I. Flege, F. Mauss, Reaction mechanism development for methane steam reforming on a Ni/Al_2O_3 catalyst, Catalysts 13 (2023) 884, https://doi.org/10.3390/catal13050884.
[23] S.N. Miskan, B.A. Abdulkadir, B. Abdullah, S.A.F. Syed, S.B. Muhammad, H. D. Ismail Setiabudi, Mini-review on fibrous zeolite catalysts for CO2 reforming of methane, Mater. Today Proc. (2023) S2214785323044218, https://doi.org/10.1016/j.matpr.2023.08.155.
[24] Z. He, J. De Wilde, Numerical simulation of commercial scale autothermal chemical looping reforming and bi-reforming for syngas production, Chem. Eng. J. 417 (2021) 128088, https://doi.org/10.1016/j.cej.2020.128088.
[25] J. Boon, Sorption-enhanced reactions as enablers for CO_2 capture and utilisation, Curr. Opin. Chem. Eng. 40 (2023) 100919, https://doi.org/10.1016/j.coche.2023.100919.
[26] H. Zheng, X. Jiang, Y. Gao, A. Tong, L. Zeng, Chemical looping reforming: process fundamentals and oxygen carriers, Discov. Chem. Eng. 2 (2022) 5, https://doi.org/10.1007/s43938-022-00012-3.
[27] A. Zaabout, S. Cloete, M. Van Sint Annaland, F. Gallucci, S. Amini, Experimental demonstration of control strategies for a Gas Switching Combustion reactor for power production with integrated CO_2 capture, Chem. Eng. Res. Design 111 (2016) 342–352, https://doi.org/10.1016/j.cherd.2016.05.007.
[28] M.H. Akbari, A.H.S. Ardakani, M.A. Tadbir, A microreactor modeling, analysis and optimization for methane autothermal reforming in fuel cell applications, Chem. Eng. J. 166 (2011) 1116–1125, https://doi.org/10.1016/j.cej.2010.12.044.
[29] Dry reforming of methane: Influence of process parameters—A review - ScienceDirect, (n.d.). https://www.sciencedirect.com/science/article/pii/S1364032115001148 (accessed November 4, 2024).
[30] R. Mansoor, M. Tahir, Recent developments in natural gas flaring reduction and reformation to energy-efficient fuels: a review, Energy Fuels 35 (2021) 3675–3714, https://doi.org/10.1021/acs.energyfuels.0c04269.
[31] D. Pashchenko, Experimental investigation of synthesis gas production by methane reforming with flue gas over a NiO-Al_2O_3 catalyst: Reforming characteristics and pressure drop, Int. J. Hydrogen Energy 44 (2019) 7073–7082, https://doi.org/10.1016/j.ijhydene.2019.01.250.
[32] Y. Cao, H. Zhang, X. Liu, Q. Jiang, H. Hong, A strategy of mid-temperature natural gas based chemical looping reforming for hydrogen production, Int. J. Hydrogen Energy 47 (2022) 12052–12066, https://doi.org/10.1016/j.ijhydene.2022.01.231.
[33] Novel ways for hydrogen production based on methane steam and dry reforming integrated with carbon capture, Energy Convers. Manage. 270 (2022) 116199. https://doi.org/10.1016/j.enconman.2022.116199.
[34] W.Y. Lee, J. Hanna, A.F. Ghoniem, On the predictions of carbon deposition on the nickel anode of a SOFC and its impact on open-circuit conditions, J. Electrochem. Soc. 160 (2013) F94–F105, https://doi.org/10.1149/2.051302jes.
[35] S. Nagpal, C.H. Lee, N. Sitapure, Y. Kim, Z. Gagnon, J.-S.-I. Kwon, Multiscale modeling of catalyst deactivation in dry methane reforming, Chem. Eng. J. 499 (2024) 155846, https://doi.org/10.1016/j.cej.2024.155846.
[36] B. Delley, From molecules to solids with the DMol3 approach, J. Chem. Phys. 113 (2000) 7756–7764, https://doi.org/10.1063/1.1316015.
[37] W. Chen, S. Liu, M. Cao, C. Lu, Y. Xu, J. Li, Adsorption of methanol and methoxy on Cu(111) surface: a first-principles periodic density functional theory study, Chin. J. Chem. 24 (2006) 872–876, https://doi.org/10.1002/cjoc.200690166.
[38] M.H. Rasmussen, J.H. Jensen, Fast and automatic estimation of transition state structures using tight binding quantum chemical calculations, (n.d.).
[39] W. Li, Z. Wang, X. Xiao, Z. Zhang, A. Janotti, S. Rajasekaran, B. Medasani, Predicting band gaps and band-edge positions of oxide perovskites using density functional theory and machine learning, PhysRevB 106 (2022) 155156, https://doi.org/10.1103/PhysRevB.106.155156.
[40] S. Sitha, Better performance of Hartree–Fock over DFT: a quantum mechanical investigation on pyridinium benzimidazolate types of zwitterions in the light of localization/delocalization issues, J. Mol. Model. 29 (2023) 313, https://doi.org/10.1007/s00894-023-05706-1.
[41] Q.S. Fu, J. Chen, Z.X. Yu, R.S. Yang, Study on the structures and surface forces of different carbon blacks by atomic force microscopy, AMM 496–500 (2014) 106–109, https://doi.org/10.4028/www.scientific.net/AMM.496-500.106.
[42] K. Barati, Y. Khojasteh-Salkuyeh, O. Ashrafi, P. Navarri, Electrified combined reforming of methane process for more effective CO_2 conversion to methanol: process development and environmental impact assessment, Energ. Conver. Manage. 287 (2023) 117096, https://doi.org/10.1016/j.enconman.2023.117096.
[43] Z. Zong, N. Koers, G. Cai, D.C. Upham, CO_2-to-methanol: Economic and environmental comparison of emerging and established technologies with dry reforming and methane pyrolysis, Chem. Eng. J. 487 (2024) 150274, https://doi.org/10.1016/j.cej.2024.150274.